



Microfluidic mixing using PDMS-based microporous structures

Dongdong Liu¹ · Tuan Tran¹

Received: 24 June 2018 / Accepted: 4 October 2018 / Published online: 19 October 2018
© Springer-Verlag GmbH Germany, part of Springer Nature 2018

Abstract

We showed that efficient mixing of fluid flows at microscales can be achieved by a simple type of micromixers based on microporous structures. We used sugar particles as templates for fabricating the microporous structures. We quantitatively studied the relation between the mixing performance and the characteristics of the microporous structures, and showed that permeability is the key indicator of the mixing performance. By visualizing the flow inside the microstructures using confocal microscope, we also found that flow passage having repetitive and sudden contraction–expansion is the chief factor leading to mixing enhancement.

Keywords Microfluid · Micromixing · Microporous

1 Introduction

Efficient and rapid mixing of fluids has been an intrinsic challenge in microfluidic applications (Stone et al. 2004; Nguyen and Zhigang 2004; Whitesides 2006), e.g., biological processes and chemical reactions (Nguyen and Zhigang 2004; Janoschka et al. 2015; Noack et al. 2015) in which minute amounts of fluids are handled in microchannels. Besides working as independent devices for rapid fluid mixing, the micromixers can also be integrated into a microfluidic system, e.g., biochemistry analysis. With small characteristic length scales ranging from 10^1 to 10^3 μm and limited flow rates, or equivalently small Reynolds numbers varying from 10^{-3} to 10^2 (Nguyen and Zhigang 2004), mixing of fluids flowing in these channels is slow and inefficient as it is dominated by diffusion.

To address this problem, numerous devices used exclusively for mixing of fluids in microfluidic applications have been devised. Typically, these devices are categorized into active and passive micromixers (Ward and Fan 2015). Active micromixers utilize flow disturbances induced by motion of active elements caused by external forces. Examples of active micromixers found to substantially enhance the

mixing efficiency include those utilizing micro-pillars actuated by magnetic force (Yu et al. 2016; Hejazian et al. 2016), inlet velocity instability imposed by electric field (Yupan et al. 2017; Shang et al. 2016), and vibration induced by acoustic field (Huang et al. 2013; Van Phan et al. 2015; Huang et al. 2015; Bachman et al. 2018; Huang et al. 2018). With sufficient input power and suitable design of structures in microchannels, high mixing performance can be achieved even with relatively short channel length.

Passive micromixers, on the other hand, can be operated without external power input. This is a desirable feature for easy integration of such micromixers into more complex systems (Nguyen and Zhigang 2004), or those having sensitive elements such as living cells (Sudarsan Arjun and Ugaz 2006). However, passive micromixers often require complex structures to create secondary flows or chaotic flows inside microchannels. Examples of such passive micromixers include those utilizing spiral (Sudarsan Arjun and Ugaz 2006) and meandering microchannels (Ahn et al. 2008). This type of micromixer requires microchannels of large lengths due to relatively weak secondary flow. Crosswise grooves were used in microchannels to generate chaotic advection and intensify mass exchange between two fluids (Stroock et al. 2002). In addition, stacked micromixers (Ritter et al. 2016; Sudarsan and Ugaz 2006) consisting of several layers of microchannels were used to enhance flow circulation and separation. Several of these micromixers can be connected in a row to further increase the mixing efficiency. Nonetheless, an apparent drawback of existing passive

✉ Tuan Tran
ttran@ntu.edu.sg

¹ School of Mechanical and Aerospace Engineering,
Nanyang Technological University, 50 Nanyang Avenue,
Singapore 639798, Singapore

micromixers is the extensive fabrication efforts required to create complex structures or to incorporate sub-components into microchannels.

To reduce the efforts required in design and fabrication of complex structures while still maintaining high mixing efficiency (Nguyen and Zhigang 2004), random and complex network of fluid passages in porous media may be utilized in fabrication of passive micromixers. Such a method has been widely used in various engineering applications, e.g., chemical reactor engineering, energy storage and recovery (Scheidegger 1958; Nield et al. 2006). Porous structures with sufficiently small pores may bring viscous dominating flows in microchannels to inertial controlling flows at low Reynolds numbers, i.e., from 10^{-3} to 10^2 (Nguyen and Zhigang 2004). In particular, polydimethylsiloxane (PDMS) porous media fabricated with sugar particles as templates were utilized for various microfluidic applications, e.g., gas generation and absorption reactions (Yuen and DeRosa 2011), oil adsorption (Si et al. 2015), micropumping (Linfeng et al. 2015), and storage and release of aqueous solutions (Thurgood et al. 2017). Furthermore, functionalizing such media using inorganic nanomaterial creates inorganic–organic composites, which inherit properties of inorganic nanomaterial and elasticity of organic polymer. These composite materials are of great engineering and industrial interests since nanomaterial additives are capable of substantially enhancing mechanical, wetting, and conductive properties of the materials (Han et al. 2013; Tran et al. 2015; Liang et al. 2016; Qiu et al. 2017).

In this study, we demonstrated fabrication and utilization of micromixers made of PDMS-based structures with varying pore size. We used sugar particles of two nominal sizes, 120 μm and 440 μm , to fabricate porous media of different pore sizes in the mixing chambers of the micromixers. We characterized the mixing chambers optically using confocal microscopy and quantitatively by measuring the permeability. Finally, we evaluated and compared the mixing performance of all the micromixers for a wide range of flow rates, from 40 to 320 $\mu\text{l} \cdot \text{min}^{-1}$.

2 Methods

2.1 Fabrication of the micromixers

Each one of our micromixers consisted of two main components: microchannels and a mixing chamber with interconnected microstructures inside. First, we fabricated a polymethyl methacrylate (PMMA) mold of a “T”-shaped junction joining two inlets and a mixing chamber. The two inlets were 400 μm in width and 640 μm in depth (Fig. 1a), while the mixing chamber of 1600 μm in width and 1800 μm in length. We casted a mixed polydimethylsiloxane (PDMS)

precursor with a mixing ratio of 10:1 onto the PMMA mold. The PDMS precursor polymerized at 80 $^{\circ}\text{C}$ for 2.5 h (Fig. 1b). The interconnected microstructures were then created inside the mixing chamber.

To fabricate microstructures inside a mixing chamber, we ground sugar particles and selected two groups of sugar particles each within a narrow size distribution using two sieves. A pair of sieves with hole sizes of 50 μm and 150 μm was used for one group, while another pair with hole sizes of 250 μm and 350 μm was applied for another group. We denoted these two groups as groups “A” and “B”, respectively. The chips in group A were labelled from A1 to A4, and the chips in group B from B1 to B4. We carefully filled the chamber with sugar particles (Fig. 1b) and placed it in a Petri dish together with a drop of DI water (0.1 ml). The Petri dish was put in an oven at 40 $^{\circ}\text{C}$ for 1 h. This process facilitated bonding between neighboring sugar particles and eventually formed microporous structures (Yang et al. 2010; Si et al. 2015; Yuen et al. 2011). A PDMS precursor was carefully poured onto the sugar structures and subsequently cured in oven. After the PDMS was cured, PDMS residual around the entrance and exit of the chamber (see Fig. 1a) was carefully removed to expose the sugar structure. We then dissolved sugar in the microstructures in an ultrasonic bath of a mixture of DI water and ethanol (50 % mass ratio at 70 $^{\circ}\text{C}$) for 2 h. The resulting chip with interconnected microstructures inside the mixing chamber was finally bonded with a PDMS-coated glass slide by air-plasma surface activation and post-baking at 80 $^{\circ}\text{C}$ for 30 min.

2.2 Characterization of the micromixers

We geometrically characterized the microstructures of the mixing chambers of chip A1 and B1 using a laser scanning confocal microscopy (LSM710, Zeiss) having numerical aperture of 0.3 and an objective having 10 \times magnification and 5.2 mm working distance. We immersed the chips in a fluorescent solution made by dissolving fluorescein sodium salt (Sigma-Aldrich) in de-ionized (DI) water into final concentration of 1 mM. We then degassed the immersed chips in a vacuum chamber to make sure that the fluorescent solution filled the microstructures completely. We scan each chip filled with the fluorescent solution and show the representative images of the microstructures at different depths in Fig. 1c. The cell size in chip A1 ranged from 40 μm to 160 μm , with averaged value of 120 μm , while the averaged cell size in chip B1 was 440 μm .

The relation between the flow rate and the pressure drop of flows through porous media is described by Darcy’s law (Scheidegger 1958; Nield et al. 2006):

$$\nabla p = -\frac{\mu}{K}u, \quad (1)$$

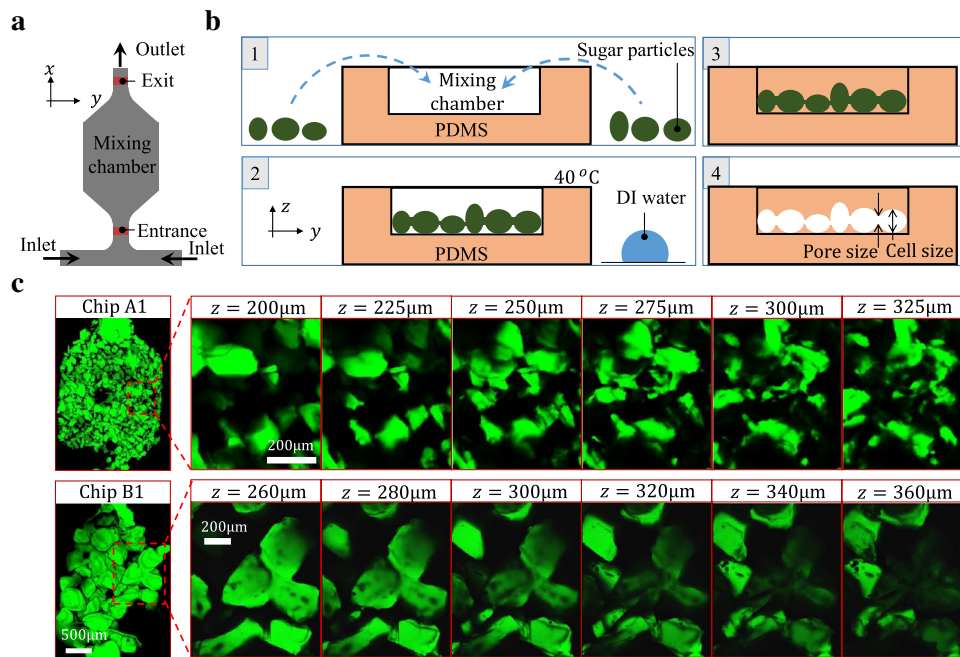


Fig. 1 **a** Schematic (not to scale) of a micromixer, which consists of two inlets and a mixing chamber. Fluorescent intensity profiles are recorded and measured at the exit of the mixing chamber (highlighted in red). **b** Fabrication process of micromixers. In step 1, an empty mixing chamber is created by casting PDMS on a PMMA mold. Subsequently, the chamber is filled with sugar particles. In step 2, the chamber filled with sugar particles and a water droplet are put in a sealed container and baked in an oven at 40 °C for 1 h to make the

particles stick to each other. In step 3, a mixture of PDMS base and curing agent is casted onto the sugar particles. In step 4, the micromixer is immersed in a hot ultrasonic bath for 2 h to dissolve sugar particles. **c** Images of the two representative chips taken at different depths by confocal microscopy showing the microstructures inside the mixing chamber. The green areas indicate hollow cells filled with fluorescent dye, while black areas are pure PMDS

where ∇p is pressure gradient in the chamber, u is characteristic velocity, μ is viscosity of a solution, and K is permeability of porous medium. This relation was obtained from the incompressible Navier–Stokes equations and is only applicable for viscous-dominated flows, or equivalently flows with sufficiently low velocity. For flows with high liquid inertia (Scheidegger 1958; Nield et al. 2006; Teng and Zhao 2000; Chai et al. 2010) or large deformation of the microstructures at high pressure (Veyskarami et al. 2016; Wang et al. 1999), the relation between the flow velocity and pressure gradient may deviate from the linear behavior.

We determined the permeability K of each chip based on measurements of the volumetric flow rate Q and pressure difference Δp between the outlet and the inlet. In Fig. 2a, we showed the dependence of Δp on Q for two representative chips, chips A1 and B1, which were fabricated with sugar particles of two nominal sizes 120 μm and 440 μm , respectively. For each chip, we noted that the pressure difference appeared to be a non-linear function of the flow rate Q due to possible deformation of PDMS microstructures (Young modulus \approx 580 kPa) in the mixing chamber (Beavers et al. 1981; Parker et al. 1987). For a fixed flow rate, we observed that the pressure difference required for chip A1 was higher, consistent with its smaller cell size (Fig. 1c). In Fig. 2b,

we showed the permeability of all tested chips; there were two groups, A and B, fabricated by sugar particles of two widely different nominal sizes, 120 μm and 440 μm , respectively. We observed that while the variation in permeability of chips in group B was rather large, from $2.0 \times 10^{-13} \text{ m}^2$ to $2.0 \times 10^{-12} \text{ m}^2$, it was much smaller for chips in group A, from $1.0 \times 10^{-13} \text{ m}^2$ to $1.8 \times 10^{-13} \text{ m}^2$, suggesting that using smaller particles results in both smaller values and smaller variations in permeability. In other words, using smaller particles in the fabrication process increased the reproducibility of chip performance.

2.3 Mixing experiment

We used aqueous solution of glycerol (G7757, Sigma-Aldrich) with 30 wt% in DI water as the stock solution. The resulting viscosity is $\mu = 2.13 \text{ mPa s}$ at 25 °C. For each chip, we used a duo-syringe pump (Legato 101, KD Scientific) to supply to one inlet with the stock solution, while the other one with fluorescent solution with concentration of 1 mM. The solutions were supplied to the inlets at the same flow rate, which ranged from 20 to 160 $\mu\text{l} \cdot \text{min}^{-1}$. The resulting total flow rate Q in the channel varied from 40 to 320 $\mu\text{l} \cdot \text{min}^{-1}$, with corresponding Reynolds number

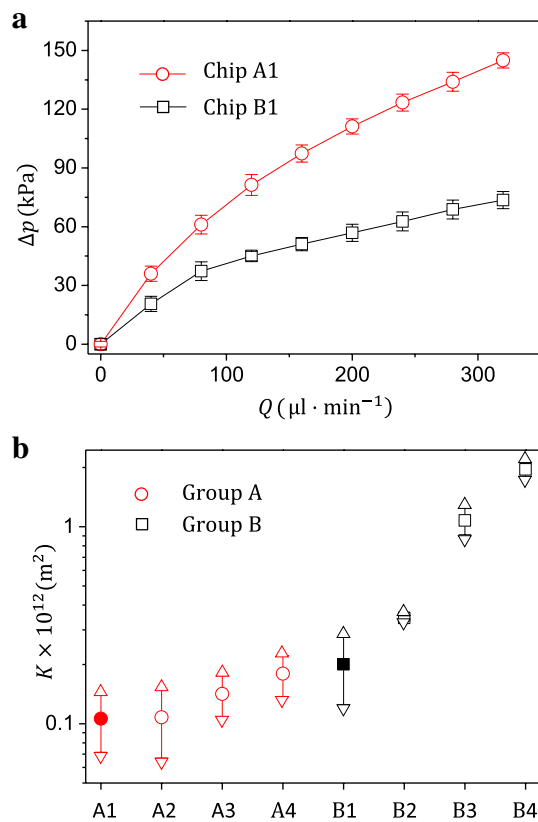


Fig. 2 **a** Variation of pressure drop Δp with flow rate Q for chip A1 and chip B1. **b** The permeability K the chips used in this study. The chips were categorized into two main groups based on the nominal size of sugar particles used in the fabrication process: group A contained chips made from nominal sugar of size $120\ \mu\text{m}$ (circles), while group B from nominal size $440\ \mu\text{m}$ (squares). For each chip, the upward and downward triangles, respectively, indicated the upper and lower limits of permeability measured at the highest ($320\ \mu\text{l} \cdot \text{min}^{-1}$) and the lowest ($40\ \mu\text{l} \cdot \text{min}^{-1}$) flow rates

$Re = \rho u D / \mu$ ranging from 0.60 to 4.82. Here D is the hydraulic diameter of the channel, u is the average velocity, ρ is the density and μ is the viscosity of the fluid.

To quantify the mixing efficiency of a micromixer, we used the intensity profile across the exit of its mixing chamber. The mixing chamber was illuminated by a mercury lamp through an excitation filter (450–490 nm). The emitted light from the micromixer passed through a long-pass filter (520 nm) and was recorded by a high-speed camera (SA5, Photron) attached to a long working-distance microscope and a $5\times$ objective (Optem). The intensity profile of the emitted light at the exit was related to the concentration profile of the solution and was used to calculate the mixing efficiency of the micromixer (Yu et al. 2016; Nguyen 2011).

The pressure drop between the inlet and the outlet of the micromixer was measured by gauge pressure sensors (Honeywell, ABP series) connected to the inlet. The measurement ranges of the sensors were from 1 to 30 psi with linearity

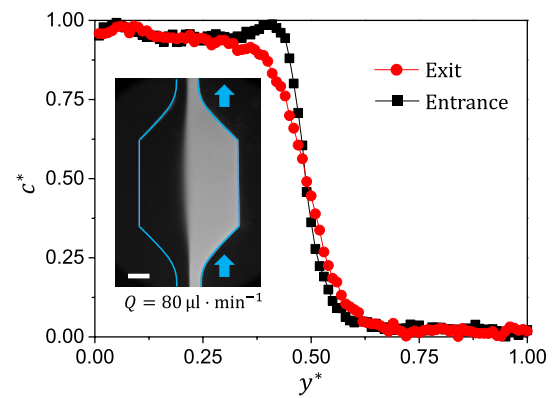


Fig. 3 Normalized intensity profile c^* measured at the entrance and exit of a mixing chamber without any microstructure. Inset: a snapshot of the mixing chamber without microstructure. The scale bar indicates $400\ \mu\text{m}$

of $\pm 1\%$. A three-way adapter was used to connect the pressure sensor to the inlet of micromixer, while the outlet was opened to ambient. The pressure measurement was conducted three times to obtain the mean value and uncertainty.

3 Results and discussion

In Fig. 3 we showed the normalized intensity profiles $c^*(y^*)$ taken from fluorescent images across the entrance and exit of the chamber fabricated without microstructures. Here $y^* = y/w$ and $c^* = (c - c_{\min}) / (c_{\max} - c_{\min})$, where c is the greyscale intensity along the transverse direction of the section selected to measure the mixing efficiency, and c_{\min} and c_{\max} , respectively, are the minimum and maximum greyscale intensities. Two feeding solutions, i.e., with and without fluorescein, were clearly separated at both the entrance and the exit of the chamber, indicating that mixing caused by the expansion in cross-sectional area at the empty mixing chamber was negligible. Using the chips with microstructures inside the mixing chamber, however, resulted in entirely different intensity profiles at the exit (Fig. 4). Qualitatively, the intensity profiles at the exit were completely levelled in chip A1 (Fig. 4a) and chip B1 (Fig. 4b) at both flow rates $80\ \mu\text{l} \cdot \text{min}^{-1}$ and $160\ \mu\text{l} \cdot \text{min}^{-1}$, suggesting that the microstructures in both chip A1 and B1 were effective in mixing the solutions supplied at the inlets.

To examine quantitatively the mixing performance of the tested chips, we measure the mixing efficiency η and show its dependence on the flow rate Q in Fig. 5. The mixing efficiency η was obtained by calculating the standard deviation of the normalized intensity profile c^* at the exit: $\eta = 1 - \langle (c^* / \langle c^* \rangle - 1)^2 \rangle^{1/2}$, where $\langle \rangle$ indicates averaging across the profile (Yu et al. 2016). While the mixing efficiencies of chips in group A were consistently high, ranging

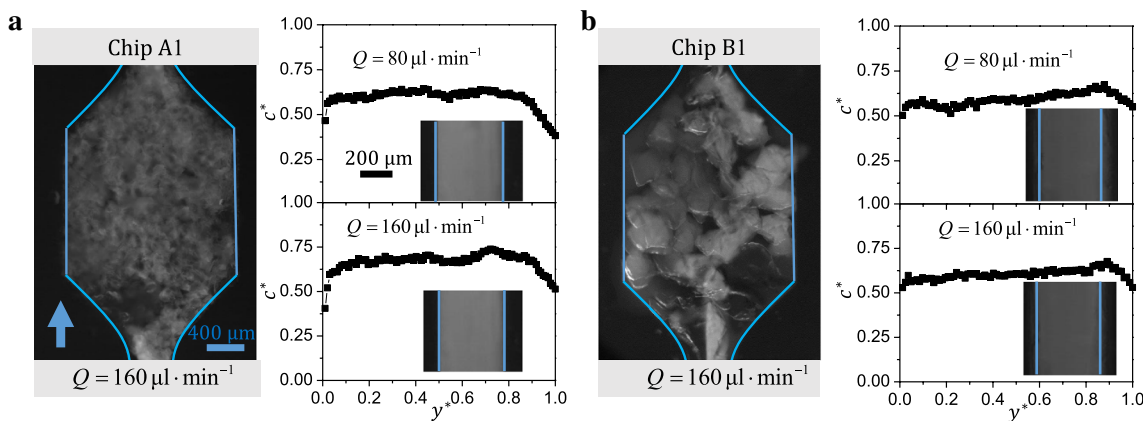


Fig. 4 Snapshots and intensity plots of mixing chambers of chip A1 (a) and chip B1 (b). Each snapshot was taken by fluorescent microscopy when the inlets of the mixing chamber are, respectively, fed with a stock solution and a fluorescent solution at the flow rate $160 \mu\text{l} \cdot \text{min}^{-1}$. For each snapshot, the normalized intensity profiles

c^* measured at the exit of the mixing chamber for two flow rates ($80 \mu\text{l} \cdot \text{min}^{-1}$ and $160 \mu\text{l} \cdot \text{min}^{-1}$) were showed. Inset of each plot was the corresponding fluorescent image used to extract the intensity profile. The arrow in figure a indicated the flow direction

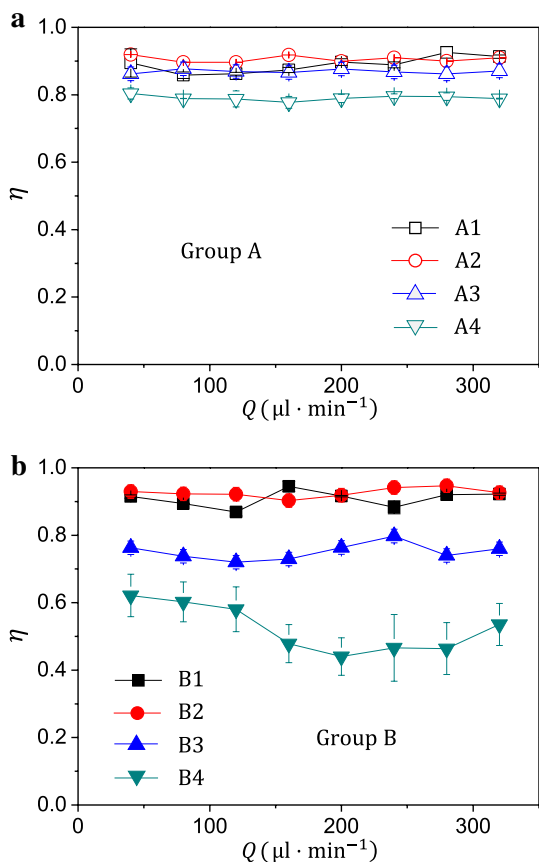


Fig. 5 Mixing efficiency η vs. volumetric flow rate Q for all micro-mixers in groups A (a) and B (b)

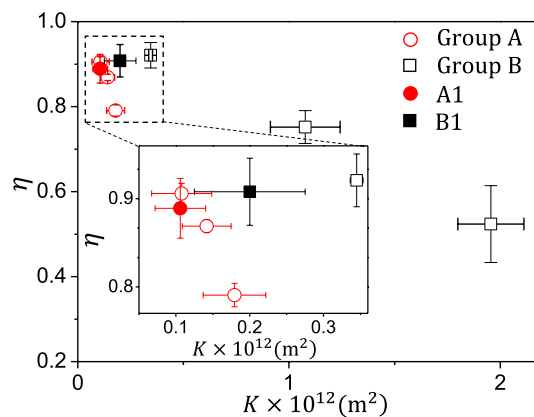


Fig. 6 Dependence of mixing efficiency η on permeability K for all the chips. The error bars represented the variation ranges of η and K

from 0.78 to 0.92, those in group B vary in a wider range, from 0.46 to 0.95. Nonetheless, we noted that the permeability of the chips with high mixing efficiency of group B (chips B1 and B2) were comparable to the permeability of those in group A (Fig. 2). This result suggested that the permeability is a key indicator of the mixing efficiency performance. Indeed, from the dependence of mixing efficiency on permeability shown in Fig. 6 for all tested chips, we observed that for each group η increases with decreasing K . It was worth noting that although low permeability correlated to high mixing efficiency, more consistent behavior was realized in group A, i.e., chips fabricated with smaller sugar particles.

We further explored the difference in mixing behaviors of chips from groups A and B by comparing the permeabilities of two chips with similar mixing efficiency: chip A2 of group A with $\eta = 0.91$, and chip B2 of group B

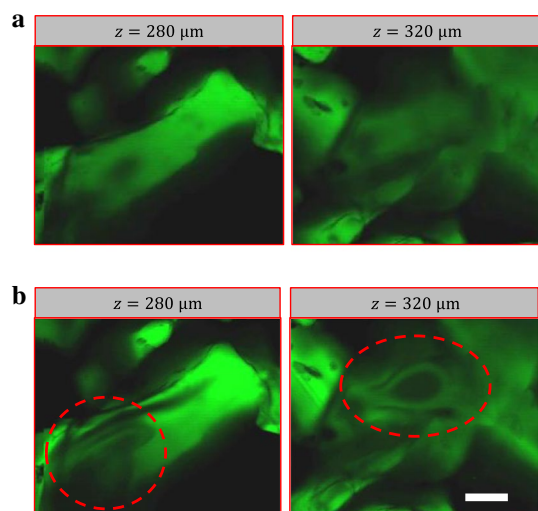


Fig. 7 **a** Representative images taken by confocal microscopy showing microstructures inside the mixing chamber of chip B1. The microstructure of the chip was filled by fluorescent solution. **b** Images taken at the same depth and viewed as those in **a**; the only difference was that one inlet of chip B1 was fed with the stock solution and the other the fluorescent solution. The different feeding solutions showed the flow patterns caused by mixing inside chip B1. The flow rate in this experiment was $160 \mu\text{l} \cdot \text{min}^{-1}$. The scale bar is $100 \mu\text{m}$

with $\eta = 0.92$. We noted that the permeability of chip A2 was $1.08 \times 10^{-13} \text{ m}^2$, almost one third of that of chip B2 ($3.45 \times 10^{-13} \text{ m}^2$). This implied that higher pressure was required to achieve the same value of η using chips made of smaller cells (group A, due to smaller size of sugar particles). Thus, higher reproducibility in chip performance, *i.e.*, low variance in K , comes at the expense of larger energy input, *i.e.*, higher operating pressure.

The difference between chips from groups A and B came from the geometrical configuration of the microstructures and the resulting flow patterns. For a particular chip, the fluid patterns inside the mixing chamber can be revealed using confocal microscopy by feeding an inlet with a fluorescent solution and the other one alternatively between the fluorescent solution and the stock solution of chip B1 are highlighted in Fig. 7b, clearly indicating circulative flows in the observed cells. These circulations may result from sudden contraction followed by expansion as the fluid passes from one cell to the other through a pore (see Fig. 1b for illustration of the pore and cell). Furthermore, we noted that although a single contraction–expansion flow passage might have a limited effect on Newtonian fluid mixing (Gan et al. 2007), a series of such passages were shown to enhance significantly mixing at low Reynolds number (from 10^{-1} to 10^2) (Ritter et al. 2016; Chen and Li 2017). Thus, the observed enhancement in mixing in chip B1 might result

from series of contraction–expansion flow passages in the microstructures. On the other hand, similar circulative flow patterns were not observed in chip A1, suggesting a different dominant mixing mechanism for flows going through smaller cells of the microstructures in chip A1. Although mass convection in individual cells might be limited, smaller cell size significantly increased the effective diffusion area and subsequently enhanced the mixing efficiency.

4 Conclusions

In summary, we presented the fabrication procedure and detailed characterization of micromixers made of PDMS-based porous media using sugar particles as microstructure templates. We focused on two groups of chips fabricated with sugar particles of nominal sizes around $120 \mu\text{m}$ and $440 \mu\text{m}$. We showed that using sugar particles with smaller size produces micromixer with both low permeability and smaller variation in permeability, thus resulting in better mixing efficiency, higher reproducibility, and more consistent mixing performance. The permeability of a chip is a key indicator for the mixing performance: for micromixers made of the same sugar size, lower permeability produces higher mixing efficiency. It was interesting, however, to note that comparing two chips of the same mixing efficiency, the one produced by larger sugar size had higher permeability, thus required smaller pressure gradient. We used confocal microscopy to reveal that this effect might result from circulative flows generated by sudden contraction–expansion flow passages in microstructures made of large cells. The results from this study might serve as a guideline to fabricate low-cost high-efficiency micromixers in microfluidic applications.

Acknowledgements This work was supported by the Nanyang Technological University (NTU) and A*STAR, Singapore. D. Liu acknowledges the research fellowship supported by A*STAR.

References

- Stone HA, Stroock AD, Ajdari A (2004) Engineering flows in small devices: microfluidics toward a lab-on-a-chip. *Annu Rev Fluid Mech* 36:381–411
- Nguyen N-T, Zhigang W (2004) Micromixers review. *J Micromechanics Microengineering* 15(2):R1
- Whitesides GM (2006) The origins and the future of microfluidics. *Nature* 442(7101):368
- Janoschka T, Martin N, Martin U, Friebe C, Morgenstern S, Hiller H, Hager MD, Schubert US (2015) An aqueous, polymer-based redox-flow battery using non-corrosive, safe, and low-cost materials. *Nature* 527(7576):78–81
- Noack J, Roznyatovskaya N, Herr T, Fischer P (2015) The chemistry of redox-flow batteries. *Angew Chem Int Ed*. 54(34):9776–9809

- Ward K, Fan ZH (2015) Mixing in microfluidic devices and enhancement methods. *J Micromechanics Microengineering* 25(9):094001
- Yu H, Nguyen T-B, Ng SH, Tran T (2016) Mixing control by frequency variable magnetic micropillar. *RSC Adv* 6(14):11822–11828
- Hejazian M, Phan D-T, Nguyen N-T (2016) Mass transport improvement in microscale using diluted ferrofluid and a non-uniform magnetic field. *RSC Adv* 6(67):62439–62444
- Yupan W, Ren Y, Tao Y, Hou L, Qingming H, Jiang H (2017) A novel micromixer based on the alternating current-flow field effect transistor. *Lab Chip* 17(1):186–197
- Shang X, Huang X, Yang C (2016) Vortex generation and control in a microfluidic chamber with actuations. *Phys Fluids* 28(12):122001
- Huang P-H, Xie Y, Ahmed D, Rufo J, Nama N, Chen Y, Chan CY, Huang TJ (2013) An acoustofluidic micromixer based on oscillating sidewall sharp-edges. *Lab Chip* 13(19):3847–3852
- Van Phan H, Bulut Coşkun M, Şeşen M, Pandraud G, Neild A, Alan T (2015) Vibrating membrane with discontinuities for rapid and efficient microfluidic mixing. *Lab Chip* 15(21):4206–4216
- Huang P-H, Chan CY, Li P, Nama N, Xie Y, Wei C-H, Chen Y, Ahmed D, Huang TJ (2015) A spatiotemporally controllable chemical gradient generator via acoustically oscillating sharp-edge structures. *Lab Chip* 15(21):4166–4176
- Bachman H, Huang P-H, Zhao S, Yang S, Zhang P, Fu H, Jun Huang T (2018) Acoustofluidic devices controlled by cell phones. *Lab Chip* 18(3):433–441
- Huang P-H, Chan CY, Li P, Wang Y, Nama N, Bachman H, Huang TJ (2018) A sharp-edge-based acoustofluidic chemical signal generator. *Lab Chip* 18(10):1411–1421
- Sudarsan Arjun P, Ugaz Victor M (2006) Multivortex micromixing. *Proc Natl Acad Sci* 103(19):7228–7233
- Ahn Y-C, Jung W, Chen Z (2008) Optical sectioning for microfluidics: secondary flow and mixing in a meandering microchannel. *Lab Chip* 8(1):125–133
- Stroock AD, Dertinger SKW, Ajdari A, Mezić I, Stone HA, Whitesides GM (2002) Chaotic mixer for microchannels. *Science* 295(5555):647–651
- Ritter P, Osorio-Nesme A, Delgado A (2016) 3d numerical simulations of passive mixing in a microchannel with nozzle-diffuser-like obstacles. *Int J Heat Mass Transf* 101:1075–1085
- Scheidegger A (1958) *The physics of flow through porous media*. University of Toronto Press, London
- Sudarsan AP, Ugaz VM (2006) Fluid mixing in planar spiral microchannels. *Lab Chip* 6(1):74–82
- Nield DA, Bejan A, Nield-Bejan (2006) *Convection in porous media*, vol 3. Springer, New York
- Yuen PK, DeRosa ME (2011) Flexible microfluidic devices with three-dimensional interconnected microporous walls for gas and liquid applications. *Lab Chip* 11(19):3249–3255
- Si P, Wang J, Zhao C, Heng X, Yang K, Wang W (2015) Preparation and morphology control of three-dimensional interconnected microporous pdms for oil sorption. *Polym Adv Technol* 26(9):1091–1096
- Linfeng X, Lee H, Jetta D, Oh KW (2015) Vacuum-driven power-free microfluidics utilizing the gas solubility or permeability of polydimethylsiloxane (pdms). *Lab chip* 15(20):3962–3979
- Thurgood P, Baratchi S, Szydzik C, Mitchell A, Khoshmanesh K (2017) Porous pdms structures for the storage and release of aqueous solutions into fluidic environments. *Lab Chip* 17(14):2517–2527
- Han J-W, Kim B, Li J, Meyyappan M (2013) Flexible, compressible, hydrophobic, floatable, and conductive carbon nanotube-polymer sponge. *Appl Phys Lett* 102(5):051903
- Tran DNH, Kabiri S, Sim TR, Losic D (2015) Selective adsorption of oil-water mixtures using polydimethylsiloxane (pdms)-graphene sponges. *Environ Sci Water Res Technol* 1(3):298–305
- Liang S, Li Y, Yang J, Zhang J, He C, Liu Y, Zhou X (2016) 3d stretchable, compressible, and highly conductive metal-coated polydimethylsiloxane sponges. *Adv Mater Technol* 1(7):1600117
- Qiu S, Bi H, Xiaohui H, Mingbo W, Li Y, Sun L (2017) Moldable clay-like unit for synthesis of highly elastic polydimethylsiloxane sponge with nanofiller modification. *RSC Adv* 7(17):10479–10486
- Yang W, Nam YG, Lee B-K, Han K, Kwon TH, Kim DS (2010) Fabrication of a hydrophilic poly (dimethylsiloxane) microporous structure and its application to portable microfluidic pump. *Jpn J Appl Phys* 49(6S):06GM01
- Yuen PK, Hui S, Goral VN, Fink KA (2011) Three-dimensional interconnected microporous poly (dimethylsiloxane) microfluidic devices. *Lab Chip* 11(8):1541–1544
- Teng H, Zhao TS (2000) An extension of darcy's law to non-stokes flow in porous media. *Chem Eng Sci* 55(14):2727–2735
- Chai Z, Shi B, Jianhua L, Guo Z (2010) Non-darcy flow in disordered porous media: a lattice boltzmann study. *Comput Fluids* 39(10):2069–2077
- Veyskarami M, Hassani AH, Ghazanfari MH (2016) Modeling of non-darcy flow through anisotropic porous media: role of pore space profiles. *Chem Eng Sci* 151:93–104
- Wang X, Thauvin F, Mohanty KK (1999) Non-darcy flow through anisotropic porous media. *Chem Eng Sci* 54(12):1859–1869
- Beavers GS, Wittenberg K, Sparrow EM (1981) Fluid flow through a class of highly-deformable porous media. part II: experiments with water. *J Fluids Eng* 103(3):440–444
- Parker KH, Mehta RV, Caro CG (1987) Steady flow in porous, elastically deformable materials. *J Appl Mech* 54(4):794–800
- Nguyen N-T (2011) *Micromixers: fundamentals, design and fabrication*. William Andrew, Norwich
- Gan HY, Lam YC, Nguyen NT, Tam KC, Yang C (2007) Efficient mixing of viscoelastic fluids in a microchannel at low reynolds number. *Microfluid Nanofluidics* 3(1):101–108
- Chen X, Li T (2017) A novel passive micromixer designed by applying an optimization algorithm to the zigzag microchannel. *Chem Eng J* 313:1406–1414

Publisher's Note Springer Nature remains neutral with regard to jurisdictional claims in published maps and institutional affiliations.